https://dx.doi.org/10.1016/j.wavemoti.2019.04.005

On the reflection and diffraction of carbon nanotube array thin film

S.K. Lai[a,b,*], L.H. Tong[c], C.W. Lim[d,e]

[a] *Department of Civil and Environmental Engineering, The Hong Kong Polytechnic University, Hung Hom, Kowloon, Hong Kong, P.R. China*

[b] *The Hong Kong Polytechnic University Shenzhen Research Institute, Shenzhen, P.R. China*

[c] *Jiangxi Key Laboratory of Infrastructure Safety and Control in Geotechnical Engineering, East China Jiaotong University, Nanchang, Jiangxi, P.R. China*

[d] *Department of Architecture and Civil Engineering, City University of Hong Kong, Tat Chee Avenue, Kowloon, Hong Kong, P.R. China.*

[e] *City University of Hong Kong Shenzhen Research Institute, Shenzhen, P.R. China*

Abstract

A theory for determining the effective refraction index of carbon nanotube array thin film is developed based on Fresnel's equation of wave normals. Here, the theory of a metallic film is used to determine the reflectivity and then to analyze the results of previous experiments on the optical properties of vertically aligned carbon nanotube arrays for different polarized incident lights. Both transverse electric-polarized lights and transverse magnetic-polarized lights are investigated, and the results agree well with the available experimental data. In a different case, when considering the weighted average of the polarized lights, the theoretical reflectivity for a non-polarized incident light is in excellent agreement with the experimental data. The refraction efficiency of a grating-patterned carbon nanotube array thin film is also investigated using the Fraunhofer diffraction theory. Based on the comparison of the theoretical and experimental results, it is concluded that the proposed theoretical model reveals the optical behavior of a carbon nanotube array thin film.

*Corresponding author. *E-mail address:* sk.lai@polyu.edu.hk (S.K. Lai)

1. Introduction

Nanomaterials and nanostructures have attracted much research attention and interest because of their unique characteristics, which are derived from their special topology and nano-metric dimensions [1]. Vertically aligned carbon nanotube (CNT) arrays can be grown on nickel-coated glass [2] or quartz substrates [3] by catalytic chemical vapor deposition. The vertically standing CNTs can be transferred, through special processing and handling, so that they are aligned parallel to the substrate surface and are also virtually parallel to each other [4]. CNT arrays in which the CNTs are grown normal and parallel to the substrates are called β-aligned CNT arrays and α-aligned CNT arrays, respectively [5]. In the past two decades, the optical characteristics of these kinds of arrays have been explored in several experimental and theoretical studies [4-13]. As the dielectric function differs for lights that are polarized parallel (s polarization) and normal (p polarization) to the CNTs, the CNT arrays display birefringent characteristics [1, 4]. Birefringent materials have an optical refractive index that depends on the polarization and propagation direction of light. To determine the effective dielectric functions of aligned CNT arrays, several methods including the Maxwell-Garnett approximation [1], effective medium approximation [5] and Fourier expansion [6] have been reported. To explain the birefringence observed by Deheer et al. [4], previous studies have mainly focused on α-aligned CNT arrays, although β-aligned CNT arrays have also attracted much recent attention. By measuring reflectivity in the visible and near infrared ranges, de los Arcos et al. [8] presented a non-destructive approach for characterizing CNT arrays and proposed a simple model for determining their thickness and porosity. Most of their models focused on the optical behavior of transverse electric (TE)-polarized light, while the transverse magnetic (TM)-polarized component was not discussed [10].

In addition to the extensive studies on the special optical properties of CNT arrays, the effects of the mirage generated by heated CNT thin films [14, 15] and the thermo-acoustics of

nano-structures and CNT thin film [16-20] have been investigated. Most recently, studies have shown that a vertically aligned CNT array is an excellent black body [21-28] capable of absorbing light from the visible to the far-infrared frequency range because of the approaching-unity effective refraction index and highly anisotropic nanoscale filamentary structure [13, 21]. CNT arrays are therefore promising candidates for application in solar cells [29], radiometers [30-32] and photonic devices [25]. The diffraction phenomena in grating-patterned [10] and circular-patterned [33] CNT array thin film have also been experimentally investigated. Hsieh et al. [10] examined the diffraction efficiency for different incident angles and detection angles, and also reported the influence of convex and concave bending of CNT array thin film on the diffraction efficiency.

In this study, the reflection of such CNT arrays is investigated theoretically for both TE- and TM-polarized lights by treating the aligned CNT arrays on a substrate as an effective uniaxial absorbing crystal. Different from previous studies, which only considered the effective ordinary or extraordinary dielectric functions [8, 25], the effective refractive indices are introduced here to study the reflectivity of the vertically aligned CNT arrays. The scattering loss caused by the rough surface, which has also been neglected in many previous studies, is shown to have a significant effect. The theoretical predictions are compared with the experimental observations for both TE- and TM-polarized lights. The reflectivity of vertically aligned CNT array thin film as a function of light incident angles is also analytically examined and compared with experimental results. It is concluded that for a 600-μm thick CNT array, the reflectivity is quite small for a large range of incident angles. The findings demonstrate that the CNT array can be used as an excellent black body absorber.

The diffraction phenomenon generated by grating-patterned CNT arrays was first observed by Hsieh et al. [10], although without a thorough theoretical analysis. Therefore, a theoretical analysis of the diffractive efficiency for this kind of grating-patterned CNT array

thin film is developed here and the theoretical prediction is compared with experimental results. The peak values of the diffraction efficiency can be predicted from the theoretical and experimental results. The overall trend is accurately and effectively revealed through the theoretical analysis derived in this work.

2. Theory and Analytical Model

2.1 Effective Dielectric of CNT Array Thin Film

A vertically aligned CNT array thin film contains a large number of CNTs that are grown normal to the substrate. To study its optical properties, the dielectric functions of the CNT array thin film should be known at the outset. A CNT array thin film can be broadly viewed as a mixture of carbon nanotubes and air. If the dielectric function of a single carbon nanotube is known, the effective dielectric functions of a CNT array thin film can be determined using the effective medium approaches [1, 34]. In general, a single CNT can be treated as a roll of graphite. Hence, it can be considered as a dielectric continuum that is locally identical to graphite. Then, the dielectric tensor of a CNT in cylindrical coordinates is [1]

$$\varepsilon(\omega) = \varepsilon_{\perp}(\omega)\left(\theta\theta + \mathbf{zz}\right) + \varepsilon_{\square}(\omega)\mathbf{rr} \tag{1}$$

where $\mathbf{r}$, θ and $\mathbf{z}$ are the cylindrical base vectors; ω is the frequency and $\varepsilon_{\perp}$ and $\varepsilon_{\square}$ are the principal components of the dielectric tensor of graphite, perpendicular and parallel to the normal axis of the graphite planes, respectively. For a vertically aligned CNT array thin film regarded as a uniaxial absorbing crystal with the optical axis $\mathbf{c}$ along the z-direction, as illustrated in Fig. 1, the dielectric functions according to the Maxwell-Garnett effective medium approach are [1, 25]

$$\varepsilon_{\perp}^{\text{eff}} = f\varepsilon_{\perp} + 1 - f \tag{2}$$

and

$$\varepsilon_{\parallel}^{\text{eff}} = \frac{\sqrt{\varepsilon_{\perp}\varepsilon_{\parallel}}(1+f)+(1-f)}{\sqrt{\varepsilon_{\perp}\varepsilon_{\parallel}}(1-f)+(1+f)} \tag{3}$$

where f is the volume fraction of CNTs, and $\varepsilon_{\perp}^{\text{eff}}$ and $\varepsilon_{\parallel}^{\text{eff}}$ are the effective dielectric functions of the CNT array thin film for an electric field **E** normal and parallel to the upper surface, i.e. parallel and normal to the optical axis, respectively.

In reality, the CNTs in the array thin film are not perfectly aligned [22, 25]. Thus, a parameter representing the obliquity of the CNTs should be introduced. The resultant effective ordinary dielectric function of the CNT array thin film can be expressed as [22, 25]

$$\varepsilon_o^{\text{eff}} = x\varepsilon_{\parallel}^{\text{eff}} + (1-x)\varepsilon_{\perp}^{\text{eff}} \tag{4}$$

For the same reason, the extraordinary dielectric function is

$$\varepsilon_e^{\text{eff}} = x\varepsilon_{\perp}^{\text{eff}} + (1-x)\varepsilon_{\parallel}^{\text{eff}} \tag{5}$$

where x specifies the contributions of the two components and $x=1$ indicates perfectly vertically aligned CNTs. The suffixes o and e stand for ordinary and extraordinary, respectively.

2.2 Effective Refractive Indices

As shown in Fig. 1, the optical axis lies in the z-direction and the unit wave normal of the incident optical wave is $\mathbf{s} = (s_x, s_y, s_z)$, in which $s_x^2 + s_y^2 + s_z^2 = 1$. As the CNT array thin film is viewed as a uniaxial crystal, three principal velocities are defined as $v_x = v_y = v_o$ and $v_z = v_e$. Fresnel's equation of wave normals can be expressed as [35]

$$\frac{s_x}{v^2 - v_o^2} + \frac{s_y}{v^2 - v_o^2} + \frac{s_z}{v^2 - v_e^2} = 0 \tag{6}$$

where v is the light velocity in the CNT array thin film. Considering $s_x^2 + s_y^2 = \sin^2\theta_i$ and $s_z^2 = \cos^2\theta_i$, where θ_i is the angle that the wave normal $\mathbf{s}$ makes with the z-axis, then Eq. (6) can be transferred into a quadratic equation with respect to v^2 as

$$\left(v^2 - v_o^2\right)\left[\left(v^2 - v_e^2\right)\sin^2\theta_i + \left(v^2 - v_o^2\right)\cos^2\theta_i\right] = 0 \tag{7}$$

The two roots of Eq. (7) are

$$\begin{aligned} v'^2 &= v_o^2 \\ v''^2 &= v_o^2\cos^2\theta_i + v_e^2\sin^2\theta_i \end{aligned} \tag{8}$$

The relation between the refractive index and light velocity is $v = c/n$, in which c is the light velocity in a vacuum and n is the refractive index. It is clear that one of these two velocities depends on the angle between the direction of the wave normal and the optical axis. For a non-magnetic CNT array thin film, the ordinary and extraordinary velocity can be obtained as $v_o^2 = c^2/\varepsilon_o^{\text{eff}}$ and $v_e^2 = c^2/\varepsilon_e^{\text{eff}}$, respectively. Substituting these two expressions into Eq. (8), the two effective refractive indices are obtained as

$$\begin{aligned} n' &= \sqrt{\varepsilon_o^{eff}} \\ n'' &= \sqrt{\frac{\varepsilon_o^{eff}\varepsilon_e^{eff}}{\varepsilon_e^{eff}\cos^2\theta_i + \varepsilon_o^{eff}\sin^2\theta_i}} \end{aligned} \tag{9}$$

The second expression in Eq. (9) indicates that the refractive index is dependent on the incident angle. These two refractive indices are different except in the special case of normal incidence ($\theta_i = 0$). Therefore, for a non-normal incident optical beam, there are always two transmitted beams in the CNT array thin film; i.e., the birefringence phenomenon occurs. Furthermore, according to the theory of crystal optics [35], each transmitted wave should obey the same law of refraction as in the case of an isotropic media. Thus,

$$\frac{\sin\theta_i}{\sin\theta_{t1}} = \frac{n'}{n_0}, \quad \frac{\sin\theta_i}{\sin\theta_{t2}} = \frac{n''}{n_0} \tag{10}$$

where n_0 is the refractive index of air, and θ_{t1} and θ_{t2} are the angles of refraction corresponding to $n^{'}$ and $n^{''}$, respectively (see Fig. 1). The angles of refraction can be determined from Eq. (10).

2.3 Reflectivity of CNT Array Thin Film

As explained in the previous section, an incident optical wave always corresponds to two transmitted optical waves for non-normal incidence in CNT array thin film. Thus, if there are two reflective optical waves that correspond to two transmitted optical waves, respectively (see Fig. 1), then the total reflectivity is assumed to be the weighted average of these two components. Because any arbitrarily polarized plane optical wave may be resolved into two waves, a TE wave and a TM wave, and these two waves are mutually independent [35], it is sufficient to study the reflectivity of TE and TM waves. A case of practical interest is a vertically aligned CNT array thin film that sits on a substrate, as illustrated in Fig. 1. The technical implication of this case is analyzed using the theory of metallic film [35]. The TE and TM waves are discussed separately.

2.3.1 TE wave

As shown in Fig. 1, digits 1, 2 and 3 stand for three media: medium 1 is air, and media 2 and 3 are the CNT array thin film and substrate, respectively. It is assumed here that the substrate is a homogenous medium with a refractive index n_3. For clarity and convenience, $n_{21} = n^{'}$, $n_{22} = n^{''}$ and n_1 is the refractive index of air. To obtain the reflectivity of the CNT array thin film, the reflection coefficients for interfaces 1-2 and 2-3 should be evaluated. As explained previously, there are two reflection coefficients for each interface. The reflection

coefficients for interfaces 1-2 and 2-3 corresponding to n_{21} according to the law of reflection [35] are

$$\overset{1}{r}_{12} = \overset{1}{\rho}_{12} e^{j\overset{1}{\phi}_{12}} = \frac{n_1 \cos\theta_i - n_{21} \cos\theta_{t1}}{n_1 \cos\theta_i + n_{21} \cos\theta_{t1}} \tag{11}$$

and

$$\overset{1}{r}_{23} = \overset{1}{\rho}_{23} e^{j\overset{1}{\phi}_{23}} = \frac{n_{21} \cos\theta_{t1} - n_3 \cos\theta_3}{n_{21} \cos\theta_{t1} + n_3 \cos\theta_3} \tag{12}$$

respectively, in which $j = \sqrt{-1}$, $\overset{1}{\rho}_{12}$ and $\overset{1}{\rho}_{23}$ are the amplitudes of the reflection coefficients, $\overset{1}{\phi}_{12}$ and $\overset{1}{\phi}_{23}$ are the phase changes and θ_3 is the angle of refraction from the thin film to the substrate. The reflection coefficients for interfaces 1-2 and 2-3 corresponding to n_{22} are similar to Eqs. (11) and (12), which can be obtained directly by replacing superscript 1 with 2 and replacing θ_{t1} and n_{21} with θ_{t2} and n_{22}, respectively. It should be noted that θ_{ti} and n_{2i} ($i = 1, 2$) are complex quantities. Accordingly, $n_1 \sin\theta_i = n_{21} \sin\theta_{t1} = n_{22} \sin\theta_{t2} = n_3 \sin\theta_3$ and the angle θ_3 can be determined by

$$\theta_3 = \arcsin \frac{n_1 \sin\theta_i}{n_3} \tag{13}$$

2.3.2 TM wave

The reflective coefficients for a TM wave can be obtained simply by replacing $n_k \cos\theta_k$ with $\cos\theta_k / n_k$ in Eqs. (11) and (12) [35]. For example, $n_1 \cos\theta_i$ and $n_{21} \cos\theta_{t1}$ should be replaced by $\cos\theta_i / n_1$ and $\cos\theta_{t1} / n_{21}$, respectively.

Once the reflective coefficients and phase changes for each interface are known, the reflectivity of a CNT array thin film can be immediately evaluated. For convenience, the following notations are defined:

$$\eta = \frac{2\pi}{\lambda} h, \quad \upsilon_{2i} = \mathrm{Im}\left(n_{2i} \cos\theta_{ti}\right), \quad u_{2i} = \mathrm{Re}\left(n_{2i} \cos\theta_{ti}\right) \tag{14}$$

where $i = 1, 2$, $\mathrm{Im}(\square)$ and $\mathrm{Re}(\square)$ denote the imaginary and real parts, respectively, λ is the wavelength and h is the thickness of the thin film. The reflectivity of the thin film may be obtained using the known quantities $\overset{1}{\rho}_{12}$, $\overset{1}{\phi}_{12}$, etc. Thus, the reflective coefficients of a CNT array thin film corresponding to n_{21} and n_{22} are [35]

$$r_1 = \rho_1 e^{j\delta_1} = \frac{\overset{1}{\rho}_{12} e^{j\overset{1}{\phi}_{12}} + \overset{1}{\rho}_{23} e^{-2\upsilon_{21}\eta} e^{j(\overset{1}{\phi}_{23} + 2u_{21}\eta)}}{1 + \overset{1}{\rho}_{12}\overset{1}{\rho}_{23} e^{-2\upsilon_{21}\eta} e^{j(\overset{1}{\phi}_{12} + \overset{1}{\phi}_{23} + 2u_{21}\eta)}} \tag{15}$$

and

$$r_2 = \rho_2 e^{j\delta_2} = \frac{\overset{2}{\rho}_{12} e^{j\overset{2}{\phi}_{12}} + \overset{2}{\rho}_{23} e^{-2\upsilon_{22}\eta} e^{j(\overset{2}{\phi}_{23} + 2u_{22}\eta)}}{1 + \overset{2}{\rho}_{12}\overset{2}{\rho}_{23} e^{-2\upsilon_{22}\eta} e^{j(\overset{2}{\phi}_{12} + \overset{2}{\phi}_{23} + 2u_{22}\eta)}} \tag{16}$$

respectively, in which, ρ_i and δ_i ($i = 1, 2$) are the amplitude and phase change, respectively. From Eqs. (15) and (16), it is observed that the phase changes of these two reflective coefficients may be different, and interference occurs for the reflective lights corresponding to n_{21} and n_{22}. Then, by taking the weighted average of r_1 and r_2, the total reflective coefficient becomes

$$r = \rho e^{i\delta} = \mu r_1 + (1 - \mu) r_2 \tag{17}$$

where μ is the weighted coefficient and $\mu = 0.5$ corresponds to the average of r_1 and r_2, and ρ and δ are the amplitude and phase change, respectively. From the total reflective coefficient, the reflectivity of the CNT thin film can be evaluated as

$$R = |r|^2 \tag{18}$$

Equations (15) to (18) are valid for both TE and TM waves. In reality, the transmissibility of a CNT array thin film can also be evaluated; however, in this study, the reflectivity rather than

the transmissibility is the main subject of analysis. Because CNT array thin film is a strong diffuser [21], the scattering loss caused by a rough surface should be considered. Hence, the effective reflectivity should be revised as [24, 35, 36]

$$R_{eff} = R \cdot \mathrm{e}^{-16\pi^2\sigma_{rms}^2 \cos^2\theta_i/\lambda^2} \tag{19}$$

in which σ_{rms} is the root-mean-square of the diffuser height.

2.4 Azimuth Angle of Reflected Light

A CNT array thin film is an effective light-absorbing material. For a thickness h with a magnitude of tens of microns or greater, the intensity of light attenuates to zero before the light reaches the interface 2-3. The reflected light is mainly attributable to the first reflected ray. The azimuth angle of the reflected light in this case is discussed here. In fact, this case is practical in many applications because most CNT array thin films are tens or hundreds of microns thick. For an linearly polarized incident light with an azimuth angle α_i, the azimuth angle of reflected light α_r satisfies the following relations [35]:

$$\tan\alpha_r = -\frac{\cos\left(\theta_i - \theta_t\right)}{\cos\left(\theta_i + \theta_t\right)}\tan\alpha_i \tag{20}$$

It is clear from Eq. (20) that for incident angle $\theta_i = 0$ (normal incidence) or $\theta_i = \pi/2$ (grazing incidence), the polarized direction of reflected light is unchanged with reference to the incident light. Moreover, the polarization of reflected light remains unchanged for azimuth angles $\alpha_i = 0$ (TM wave) and $\alpha_i = \pi/2$ (TE wave). The polarization of reflected light will change in all except these special cases.

2.5 Diffraction of Grating Patterned CNT Arrays

In general, diffraction can be observed when an incident light is normal to the grating direction [29, 30]. A grating-patterned CNT array thin film was fabricated and tested by Hsieh et al. [10] to observe this effect. Although the diffraction efficiency for different circumstances has been investigated experimentally [10], a rigorous theoretical analysis is still lacking. Hence, in this study a theoretical model is proposed and analyzed. A grating-patterned CNT array thin film is illustrated in Fig. 2. The grating period is d, the width of the grid is s and θ_0 and θ denote the incident angle and diffraction angle, respectively.

According to Fraunhofer's diffraction theory [35], the intensity of light at a point of observation P is normalized as

$$I(P)=\left[\frac{\sin(Nkdp/2)}{N\sin(kdp/2)}\right]^2\left[\frac{\sin(ksp/2)}{ksp/2}\right]^2 \tag{21}$$

in which $k=2\pi/\lambda$ is the optical wavenumber, $p=\sin\theta-\sin\theta_0$ and N is the effective number of grids illuminated by the incident optical light. Due to light absorption in a CNT thin film, the intensity of refractive light decreases along the path. Therefore, an attenuation factor should be added to Eq. (21) to account for the effect of absorption. Thus, the effective intensity of light is

$$I_{eff}(P)=\left[\frac{\sin(Nkdp/2)}{N\sin(kdp/2)}\right]^2\left[\frac{\sin(ksp/2)}{ksp/2}\right]^2\cdot e^{-2\upsilon_2\eta} \tag{22}$$

where $\upsilon_2=(\upsilon_{21}+\upsilon_{22})/2$, and η is defined in Eq. (14). It is clear that the refraction efficiency is proportional to the effective intensity of light obtained in Eq. (22).

3 Results and Discussion

To verify the theory and model proposed here, the theoretical predictions are compared with published experimental data in this section. In these examples, the optical constants of

graphite for the effective refractive index of CNT array thin film are taken from Bao et al. [9]. The weighted coefficient is $\mu = 0.5$ in the following analysis unless otherwise stated.

3.1 Reflectance of TE and TM Waves

In the experiment of Hsieh et al. [10], the CNT array thin film was grown on a silicon substrate. The thickness of the thin film used in their experiments was 2 μm. The reflectivity for different incident angles is presented for both the TE and TM waves with varying wavelengths [10]. The theoretical predictions proposed in this study are compared with the experimental results in Fig. 3 and Fig. 4 for TE and TM waves, respectively. Wang et al. [24] used atomic force microscopy to observe the surface profile of a CNT array with a thickness of $166\ \mu m$ and the root-mean-square roughness was determined as 57 nm. Because the CNT array studied here is relatively thin compared with that used by Wang et al. [24], a root-mean-square roughness of 20 nm is adopted. Scanning electron microscopy determined that the density of CNTs in a unit area ranges from 10^{11} to 10^{12} cm^{-2} [10]. Assuming that the average diameter of CNTs is 5 nm, as Garcia-Vidal et al. [1] suggested, the volume fraction may be determined as approximately 2.6% to 26%. The theoretical predictions obtained from this work are in good agreement with the experimental results for both TE and TM waves. The volume fractions taken by TE and TM waves are 0.09 and 0.065, respectively. Figs. 3(a) and 3(b) show that the oscillatory magnitude of reflectivity for a TE wave increases with increasing wavelength, due to the higher absorption capacity of CNT thin film at shorter wavelengths and to the decrease in scattering loss with increasing wavelength, as predicted by Eq. (19).

The optical properties for a TM wave are different, as shown in Fig. 4, which illustrates the optical anisotropy of CNT thin films. The reflectivity is smaller for larger incident angles, as shown in Fig. 4. An explanation is given as follows. As the direction of the electric field of the TM-polarized light becomes increasingly parallel to the optical axis, the difference between

the two effective refraction indices in Eq. (17) becomes larger. Then the absorption of the CNT thin film increases, reducing its reflectivity. Because $n_j \cos\theta_j$ is replaced by $\cos\theta_j / n_j$ (the refractive index becomes a denominator rather than a nominator) when determining the reflectivity of the TM wave, the reflectivity with respect to the incident angles for TE and TM waves is expected to behave in an opposite manner, as observed in the experiment of Hsieh et al. [10]. Fig. 4 shows that although some specific points in the experiment at an incident angle of 20 degrees differ from the theoretical prediction, the general trend is consistent. For larger incident angles, as shown in Fig. 4, the reflectance is quite small, and hence there is almost no variation.

3.2 Reflectivity for Different Incident Angles

The incident angle significantly affects the reflectivity of the CNT array thin film. Mizuno et al. [22] experimentally studied the reflectivity as a function of the incident angle. In their experiment [22], the CNT array was 600-μm thick and the volume fraction was 0.03. Here, a very thick CNT array thin film is considered and the surface roughness is taken as $\sigma_{rms} = 50\ nm$. It is common knowledge that the volume fraction cannot be determined precisely. In this work, to achieve good agreement with the experiments, the volume fraction is chosen as 0.04. The wavelength of incident light is 5 μm, and it should be emphasized that the incident light was non-polarized in the experiment of Mizuno et al. [22]. Because any arbitrarily polarized plane optical wave may be resolved into two mutually independent TE and TM waves, the reflectivity can be determined by the weighted average of the TE and TM waves for an arbitrarily non-polarized light [21]. In this work, $0.2 \times R_{TM} + 0.8 \times R_{TE}$ is chosen as the total theoretical reflectivity. The comparison with the experimental results in Fig. 5 shows good agreement. The total reflectivity increases with the increasing incident angle. The inset of Fig. 5 shows the reflectivity of the TM wave where the reflectivity reaches a minimum at the

Brewster angle of about 46°, which corresponds to an average refractive index of 1.035. It is obvious that the small refractive index is responsible for the low reflectivity of the CNT array. Furthermore, the reflectivity is quite small for a large range of incident angles. For instance, with a 600-μm thick CNT array, there is virtually zero transmissibility, and thus more than 99% of optical energy is absorbed by the CNT array for an incident angle smaller than 50°. This is why CNT arrays can be viewed as excellent black body absorbers.

3.3 Diffraction Efficiency of Grating-Patterned CNT Arrays

The diffraction phenomenon was first observed experimentally by Hsieh et al. [10] using a grating-patterned CNT array thin film. The diffraction spectra of the CNT grating were experimentally determined at a normal incidence for different detection angles. The grating period used in their experiment was 1 μm and the grid width was 0.5 μm [10]. The effective absorbing height of patterned-grating CNT thin film is taken as 1 μm to determine η in Eq. (22). Within an acceptable discrepancy, the average effective refractive index and extinction coefficient are chosen as 1.07 and 0.038, respectively, for convenience [10]. Hsieh et al. [10] reported the diffraction efficiency for detection angles of 35° and 40°. A comparison between the theoretical prediction and the experimental data is presented in Fig. 6 (data for 30° is not shown). Considering an incident optical beam with a small diameter, the effective number of grids illuminated by the incident optical light N = 5 is selected for both 35° and 40° detection angles. Good agreement is observed between the theoretical and experimental results. The theoretical result is normalized for the sake of comparison. The peak diffraction efficiency can be predicted precisely from the theory in this work. In Fig. 6, there is some disagreement for points away from the peak, which could be the result of measurement errors or other uncertainties. However, the general trend and response can be predicted quite comfortably using the theory and analytical model developed here.

4 Conclusions

Based on the Fresnel equation of wave normals, the effective refraction index of CNT array thin film, which can be viewed as a uniaxial absorbing crystal, is obtained. Considering an arbitrarily polarized plane optical wave that could be resolved into two mutually independent waves, i.e. TE and TM waves, the reflectivity of the TE and TM waves are investigated separately by applying the theory of metallic film. Comparisons between the theoretical and experimental results for both TE- and TM-polarized light within the visible and near infrared wavelength ranges indicate good agreement for these two optical waves. Both theory and experiment indicate that reflectivity increases with the incident angle for a non-polarized light. However, the reflectivity reaches a minimum at the Brewster angle of about 46° for a TM wave when using a CNT array with a height of 600 μm. The reflectivity of a 600-μm thick CNT array is less than 1% with incident angles of less than 50°, indicating that the CNT array serves as an excellent black body absorber. The diffraction efficiency of a grating-patterned CNT array thin film is also investigated theoretically by applying the Fraunhofer diffraction theory. The peak diffraction efficiency is predicted accurately and the general behavior and responses are revealed precisely through the theoretical model and analysis. In conclusion, the optical properties of vertically aligned CNT array thin film are analyzed using a theoretical approach. The theory and model are verified using the published experimental data.

Acknowledgements

The work described in this paper was supported by the Natural Science Foundation of Jiangxi (20171BAB216047) and the National Natural Science Foundation of China (Grants No. 11702095 and 11602210).

References

[1] F.J. Garcia-Vidal, J.M. Pitarke, J.B. Pendry, Effective medium theory of the optical properties of aligned carbon nanotubes, Phys Rev Lett, 78 (1997) 4289-4292.

[2] Z.F. Ren, Z.P. Huang, J.W. Xu, J.H. Wang, P. Bush, M.P. Siegal, P.N. Provencio, Synthesis of large arrays of well-aligned carbon nanotubes on glass, Science, 282 (1998) 1105-1107.

[3] Y. Murakami, S. Chiashi, Y. Miyauchi, M.H. Hu, M. Ogura, T. Okubo, S. Maruyama, Growth of vertically aligned single-walled carbon nanotube films on quartz substrates and their optical anisotropy, Chem Phys Lett, 385 (2004) 298-303.

[4] W.A. Deheer, W.S. Bacsa, A. Chatelain, T. Gerfin, R. Humphreybaker, L. Forro, D. Ugarte, Alliged carbon nanotube films: Production and optical and electronic properties, Science, 268 (1995) 845-847.

[5] W.G. Lu, J.M. Dong, Z.Y. Li, Optical properties of aligned carbon nanotube systems studied by the effective-medium approximation method, Phys Rev B, 63 (2001) 033401.

[6] X.H. Wu, L.S. Pan, H. Li, X.J. Fan, T.Y. Ng, D. Xu, C.X. Zhang, Optical properties of aligned carbon nanotubes, Phys Rev B, 68 (2003) 193401.

[7] G.L. Zhao, D. Bagayoko, L. Yang, Optical properties of aligned carbon nanotube mats for photonic applications, J Appl Phys, 99 (2006) 114311.

[8] T. de los Arcos, P. Oelhafen, D. Mathys, Optical characterization of alignment and effective refractive index in carbon nanotube films, Nanotechnology, 18 (2007) 265706.

[9] H. Bao, X.L. Ruan, T.S. Fisher, Optical properties of ordered vertical arrays of multi-walled carbon nanotubes from FDTD simulations, Opt Express, 18 (2010) 6347-6359.

[10] K.C. Hsieh, T.Y. Tsai, D.H. Wan, H.L. Chen, N.H. Tai, Using patterned carbon nanotube films with optical anisotropy to tune the diffracted color from flexible substrates, Carbon, 48 (2010) 1410-1417.

[11] Y.X. Zhou, Y.W. E, X.L. Xu, W.L. Li, H. Wang, L.P. Zhu, J.T. Bai, Z.Y. Ren, L. Wang, Angular dependent anisotropic terahertz response of vertically aligned multi-walled carbon nanotube arrays with spatial dispersion, Scientific Reports 6 (2016) 38515.

[12] M. Wasik, J. Judek, K. Switkowski, M. Zdrojek, Optical Interference Effects in Visible-Near Infrared Spectral Range for Arrays of Vertically Aligned Multiwalled Carbon Nanotubes, Acta Phys Pol A, 131 (2017) 232-236.

[13] S.J. Park, J.G. Ok, H.J. Park, K.T. Lee, J.H. Lee, J.D. Kim, E. Cho, H.W. Baac, S. Kang, L.J. Guo, A.J. Hart, Modulation of the effective density and refractive index of carbon nanotube forests via nanoimprint lithography, Carbon, 129 (2018) 8-14.

[14] A.E. Aliev, Y.N. Gartstein, R.H. Baughman, Mirage effect from thermally modulated transparent carbon nanotube sheets, Nanotechnology, 22 (2011) 435704.

[15] L.H. Tong, C.W. Lim, Y.C. Li, C.Z. Zhang, T.Q. Bui, Generation of mirage effect by heated carbon nanotube thin film, J Appl Phys, 115 (2014) 244905.

[16] L. Xiao, Z. Chen, C. Feng, L. Liu, Z.-Q. Bai, Y. Wang, L. Qian, Y. Zhang, Q. Li, K. Jiang, S. Fan, Flexible, Stretchable, Transparent Carbon Nanotube Thin Film Loudspeakers, Nano Lett, 8 (2008) 4539-4545.

[17] V. Vesterinen, A.O. Niskanen, J. Hassel, P. Helistö, Fundamental Efficiency of Nanothermophones: Modeling and Experiments, Nano Lett, 10 (2010) 5020-5024.

[18] R. Venkatasubramanian, Applied physics: Nanothermal trumpets, Nature, 463 (2010) 619-619.

[19] C.W. Lim, L.H. Tong, Y.C. Li, Theory of suspended carbon nanotube thinfilm as a thermal-acoustic source, J. Sound Vib., 332 (2013) 5451-5461.

[20] L.H. Tong, C.W. Lim, Y.C. Li, Gas-filled encapsulated thermal-acoustic transducer, ASME J. Vibration and Acoustics, 135 (2013) 051033.

[21] Z.P. Yang, L.J. Ci, J.A. Bur, S.Y. Lin, P.M. Ajayan, Experimental observation of an extremely dark material made by a low-density nanotube array, Nano Lett, 8 (2008) 446-451.

[22] K. Mizuno, J. Ishii, H. Kishida, Y. Hayamizu, S. Yasuda, D.N. Futaba, M. Yumura, K. Hata, A black body absorber from vertically aligned single-walled carbon nanotubes, P Natl Acad Sci USA, 106 (2009) 6044-6047.

[23] X.J. Wang, J.D. Flicker, B.J. Lee, W.J. Ready, Z.M. Zhang, Visible and near-infrared radiative properties of vertically aligned multi-walled carbon nanotubes, Nanotechnology, 20 (2009) 215704.

[24] X.J. Wang, L.P. Wang, O.S. Adewuyi, B.A. Cola, Z.M. Zhang, Highly specular carbon nanotube absorbers, Appl Phys Lett, 97 (2010) 163116.

[25] H. Ye, X.J. Wang, W. Lin, C.P. Wong, Z.M. Zhang, Infrared absorption coefficients of vertically aligned carbon nanotube films, Appl Phys Lett, 101 (2012) 141909.

[26] Z.-P. Yang, M.-L. Hsieh, J.A. Bur, L. Ci, L.M. Hanssen, B. Wilthan, P.M. Ajayan, S.-Y. Lin, Experimental observation of extremely weak optical scattering from an interlocking carbon nanotube array, Appl. Opt., 50 (2011) 1850-1855.

[27] H. Shi, J.G. Ok, H.W. Baac, L.J. Guo, Low density carbon nanotube forest as an index-matched and near perfect absorption coating, Appl Phys Lett, 99 (2011) 211103-211103.

[28] J. Lehman, C. Yung, N. Tomlin, D. Conklin, M. Stephens, Carbon nanotube-based black coatings, Appl Phys Rev, 5 (2018) 011103.

[29] I. Hussain, A.R. Chowdhury, J. Jaksik, G. Grissom, A. Touhami, E.E. Ibrahim, M. Schauer, O. Okoli, M.J. Uddin, Conductive glass free carbon nanotube micro yarn based perovskite solar cells, Appl Surf Sci, 478 (2019) 327-333.

[30] G. Vera-Reveles, J. Simon, E. Briones, F.J. Gonzalez, Single walled carbon nanotube bolometer coupled to a Sierpinski fractal antenna for the detection of megahertz radiation, Microw Opt Techn Let, 54 (2012) 1251-1253.

[31] D.S. Kopylova, F.S. Fedorov, A.A. Alekseeva, E.P. Gilshteyn, A.P. Tsapenko, A.V. Bubis, A.K. Grebenko, Z.I. Popov, P.B. Sorokin, Y.G. Gladush, A.S. Anisimov, A.G. Nasibulin, Holey single-walled carbon nanotubes for ultra-fast broadband bolometers, Nanoscale, 10 (2018) 18665-18671.

[32] D.M. Lattery, M. Kim, J. Choi, B.J. Lee, X.J. Wang, Effective Radiative Properties of Tilted Metallic Nanorod Arrays Considering Polarization Coupling, Scientific Reports 8 (2018) 13896.

[33] H. Butt, T. Butler, Y. Montelongo, R. Rajesekharan, T.D. Wilkinson, G.A.J. Amaratunga, Continuous diffraction patterns from circular arrays of carbon nanotubes, Appl Phys Lett, 101 (2012) 251102.

[34] D.M. Wood, N.W. Ashcroft, Effective Medium Theory of Optical-Properties of Small Particle Composites, Philos Mag, 35 (1977) 269-280.

[35] M. Born, E. Wolf, A.B. Bhatia, Principles of Optics: Electromagnetic Theory of Propagation, Interference and Diffraction of Light, Cambridge University Press, 1999.

[36] L.G. Shirley, N. George, Diffuser Radiation-Patterns Over A Large Dynamic-Range .1. Strong Diffusers, Applied Optics, 27 (1988) 1850-1861.

Figure captions

Fig.1 A CNT array thin film on a substrate and the paths of an optical beam. θ_i and θ_r are the incident and reflective angles, respectively. $\theta_{ti}\,(i=1,2)$ are the transmitted angles.

Fig.2 A grating patterned CNT array thin film.

Fig.3 Reflectivity of a 2-μm thick CNT array thin film on Si substrate of TE wave for (a) normal incidence and (b) incident angle 20°.

Fig.4 Reflectivity of a 2-μm thick CNT array thin film on Si substrate of TM wave at incident angle 20° and 60°.

Fig.5 The reflectivity as a function of incident angle for a non-polarized light. The inserted figure shows the reflectivity of TM wave.

Fig.6 Diffraction spectra of a patterned CNT thin film grating with detection angles (a) 35°, and (b) 40° at normal incidence.

List of figures

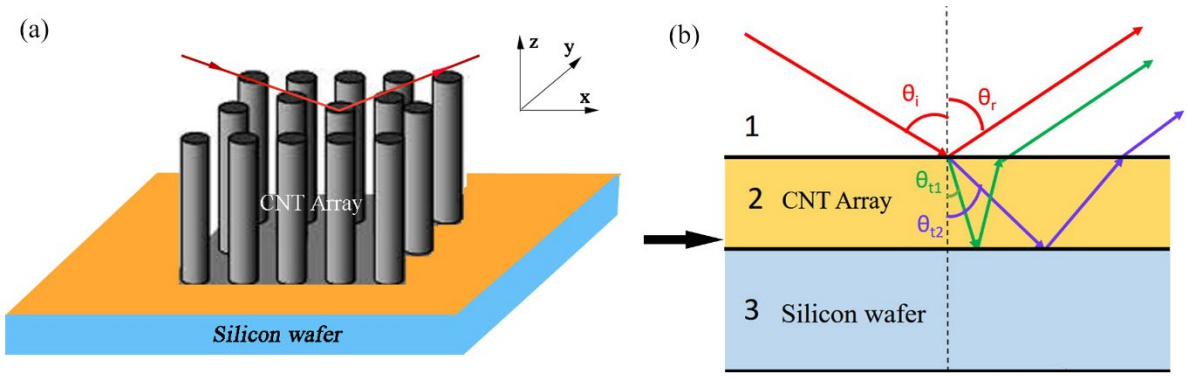

Fig.1 A CNT array thin film on a substrate and the paths of an optical beam. θ_i and θ_r are the incident and reflective angles, respectively. $\theta_{ti}\,(i=1,2)$ are the transmitted angles.

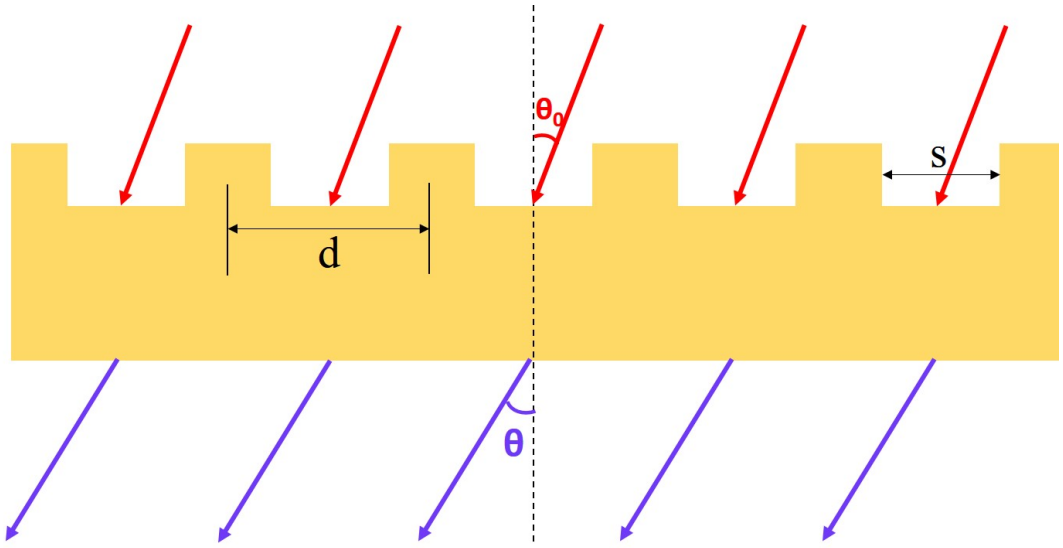

Fig.2 A grating patterned CNT array thin film.

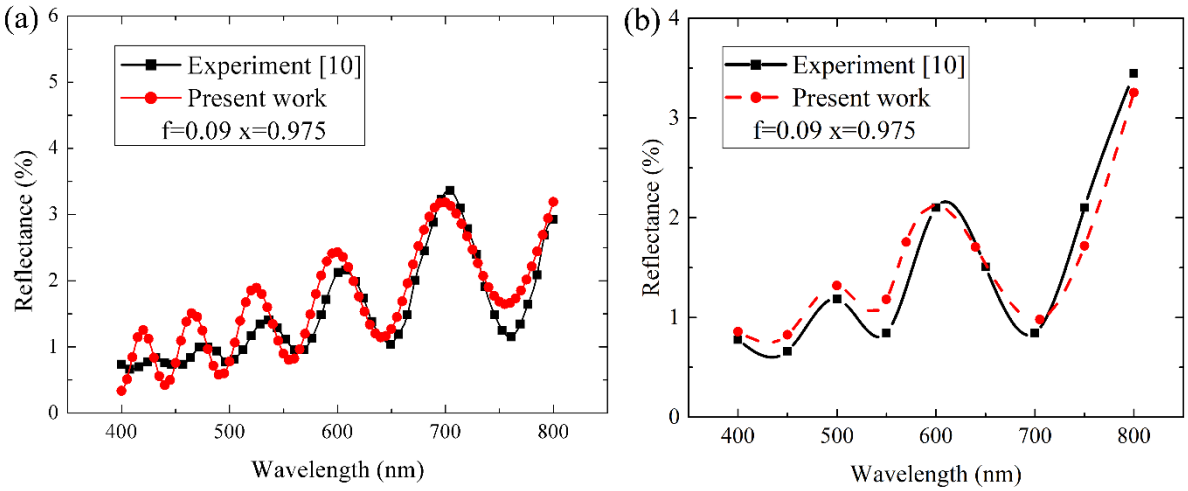

Fig.3 Reflectivity of a 2-μm thick CNT array thin film on Si substrate of TE wave for (a) normal incidence and (b) incident angle 20°.

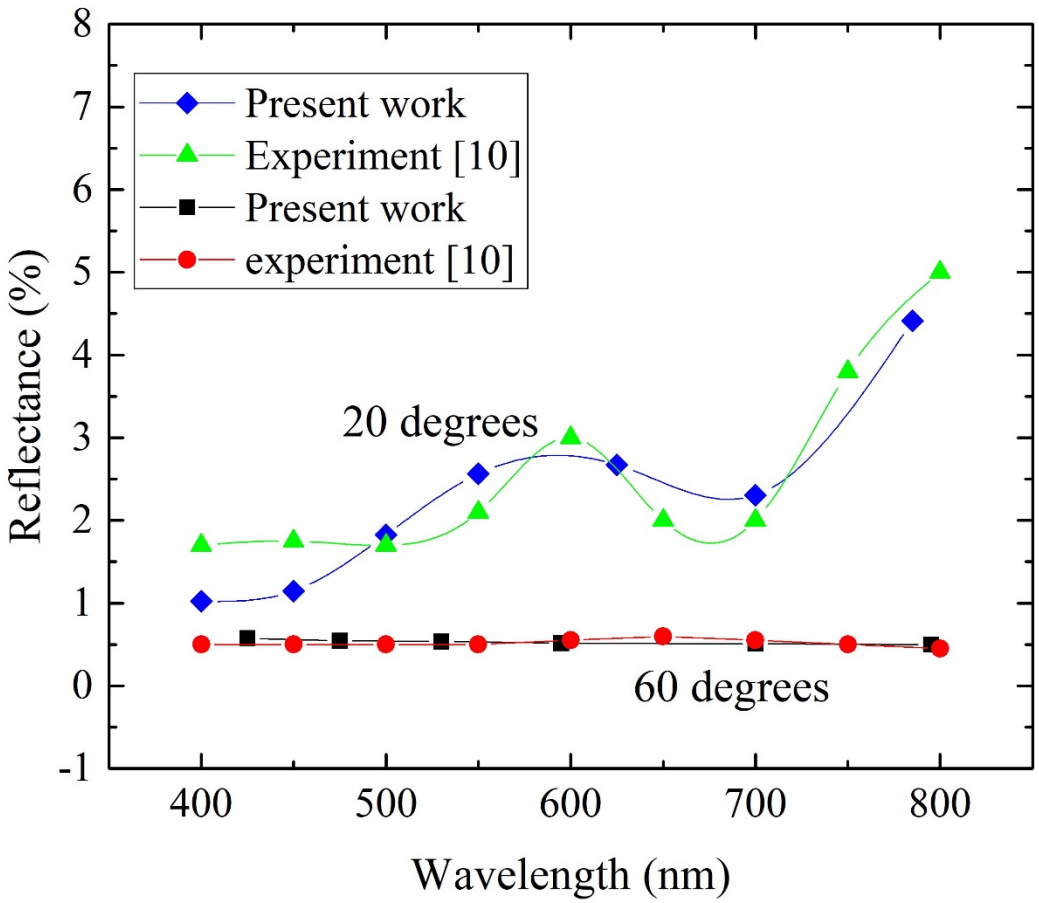

Fig.4 Reflectivity of a 2-μm thick CNT array thin film on Si substrate of TM wave at incident angle 20° and 60°.

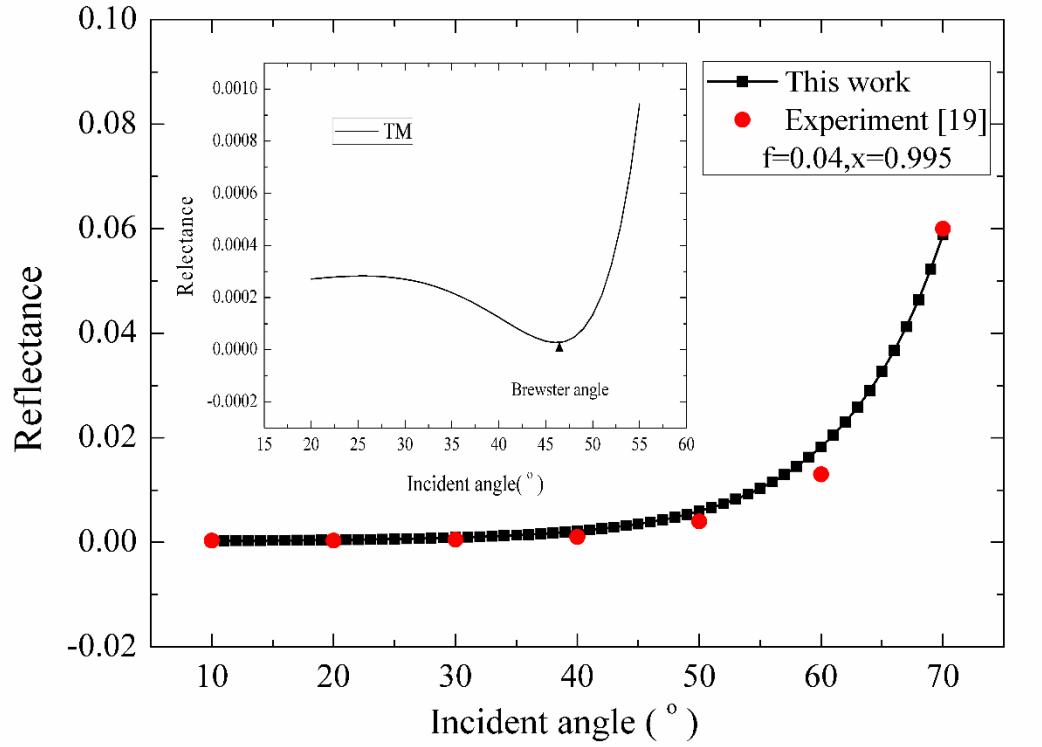

Fig.5 The reflectivity as a function of incident angle for a non-polarized light. The inserted figure shows the reflectivity of TM wave.

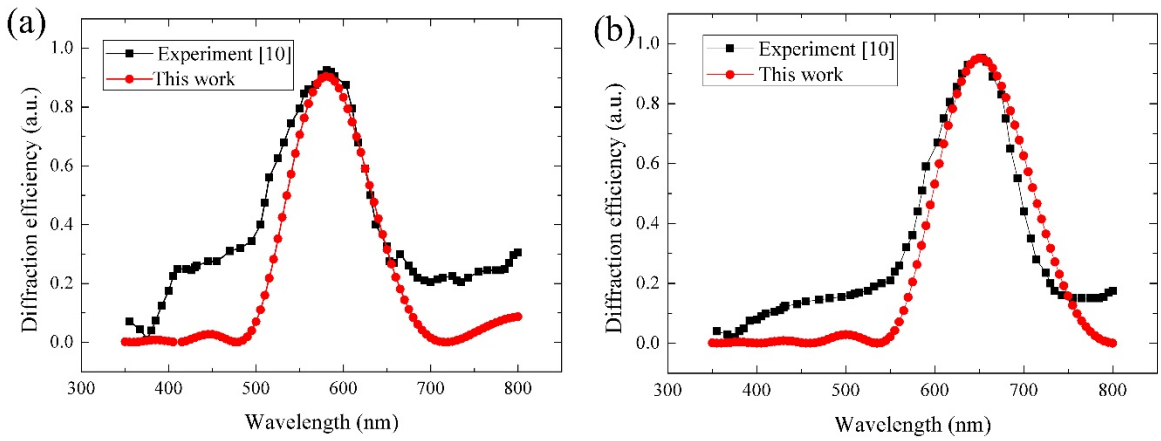

Fig.6 Diffraction spectra of a patterned CNT thin film grating with detection angles (a) 35°, and (b) 40° at normal incidence.